Int J Thermophys (2009) 30:397–415
DOI 10.1007/s10765-009-0563-9

Application of the Three-Omega Method to Measurement of Thermal Conductivity and Thermal Diffusivity of Hydrogen Gas

E. Yusibani · P. L. Woodfield · M. Fujii · K. Shinzato · X. Zhang · Y. Takata

Received: 16 April 2008 / Accepted: 21 January 2009 / Published online: 5 March 2009

Abstract Preliminary investigations have been conducted to discuss the possibility of measuring the thermal conductivity of hydrogen gas by the three-omega method. A one-dimensional analytical solution for the 3ω component is derived which includes the effect of the wire heat capacity. It is shown that it is very important to take into account the wire heat capacity in the calculation to measure the thermal conductivity of gas by the three-omega method. In contrast, the wire heat capacity is less important for the thermal conductivity of the liquid or solid phase. The importance of the

E. Yusibani (✉) · Y. Takata
Department of Mechanical Engineering, Kyushu University, Nishi-ku,
Fukuoka 819-0395, Japan
e-mail: e-yusibani@aist.go.jp

Y. Takata
e-mail: takata@mech.kyushu-u.ac.jp

P. L. Woodfield · M. Fujii · K. Shinzato
Research Center for Hydrogen Industrial Use and Strorage, National Institute
of Advanced Industrial Science and Technology (AIST), Nishi-ku,
Fukuoka 819-0395, Japan

P. L. Woodfield
e-mail: p.woodfield@aist.go.jp

M. Fujii
e-mail: fujii-motoo@aist.go.jp

K. Shinzato
e-mail: k.shinzato@aist.go.jp

X. Zhang
Key Laboratory for Thermal Science and Power Engineering of Ministry of Education,
Department of Engineering Mechanics, Tsinghua University, Beijing, China
e-mail: x-zhang@tsinghua.edu.en

wire heat capacity is found to increase with increasing frequency and decrease if the sample thermal conductivity is high. In order to measure the thermal conductivity of hydrogen gas at atmospheric pressure, a wire of diameter less than 1 μm is necessary if the properties of the wire are to be neglected.

Keywords Gas · Hydrogen · Thermal conductivity · Three-omega method

List of Symbols

A_j	Empirically determined accommodation coefficient
C_p	Heat capacity at constant pressure
f	Frequency
I_o	Magnitude of the oscillating current
I_0	Modified Bessel function of 0th order
k	Boltzmann's constant
K_0	Modified Bessel function of 0th order
K_j	The temperature-jump coefficient
K_v	Modified Bessel function of v-th order
l	Length of the wire
l_{mfp}	Mean free path
P	Pressure
Pr	Prandtl number for the gas
r_o	Radius of the wire
r	r-axis
R_T	Resistance of the wire at temperature T
R_{T0}	Resistance of the wire at temperature T at zero heating
R_{0C}	Resistance of wire at 0 °C
t	Time
T	Temperature
T_0	Initial temperature of the bath (°C)
V	Voltage
W	Power
X	Magnitude of 3ω voltage of in-phase component
Y	Magnitude of 3ω voltage of out-of-phase component
z	z-axis

Greek Symbols

α	Thermal diffusivity
σ	Effective collision cross section
β	Temperature coefficient
γ_c	The ratio of the constant-pressure specific heat to the constant-volume specific heat
λ	Thermal conductivity
ρ	Density
ω	Phase frequency ($2\pi f$)

Subscripts

fg Function generator
j Temperature jump effect
ref Reference
w Properties of the wire
s Sample

1 Introduction

The three-omega method has been widely used for measurements of the thermal conductivity/diffusivity of solids [1]. In particular, the method is well suited to thin solid films [2,3] and to situations that require very small samples. This is because the penetration depth into the sample can be reduced to the micrometer-order relatively easily by increasing the frequency of the oscillating current. Application has also been made for measurement of the thermal conductivity of carbon nanotubes [4]. In comparison with solids, fewer studies have been done with liquids although some promising results have been reported recently for nano-fluids [5] and electrically conducting liquids [6]. Also, Moon and Jeong [7] and Birge [8] used the 3ω voltage to measure the heat capacities of liquids near the glass-transition temperature. Lee [9] measured the thermal conductivity of air with the three-omega method based on the solution of Chen et al. [10] which includes wire properties.Studies related to application of the three-omega method to measurement of gas-phase properties are very scarce in the literature.

The authors of this present article are preparing for measurement of the thermal conductivity and thermal diffusivity of hydrogen gas over a wide range of temperature and pressure [11] by the transient short-hot-wire method [12]. The three-omega method appears to be an attractive alternative to the transient hot-wire method because the small penetration depth suggests that even in a very small pressure vessel it may be possible to avoid the influence of the boundary condition at the wall of the vessel. A small vessel also has advantages in terms of safety. However, assumptions in the 3ω theory related to neglect of the wire properties, natural convection effects, end effects, and temperature jump effects need confirmation in order to establish the validity of the method for gas property measurement. Cahill [1] showed that by increasing the frequency, radiation effects could be reduced for high-temperature measurement. We should expect that the same principle will apply in the case of high-temperature gas measurement. Also, end effects should decrease with an increase in frequency. Wang et al. [5] suggested that natural convection effects could be reduced in the case of liquid water by increasing the frequency of the oscillating current. However, they also showed that the properties of the wire became more important as the frequency is increased. These observations suggest that it is important to consider the different effects by simulation in order to establish a suitable range of frequencies or a suitable probe design where the 3ω method will be valid for a given fluid sample.

In the present article we focus on the effect of the heat capacity of the wire when the sample is a gas with a high diffusivity such as hydrogen at atmospheric pressure. The temperature jump will be discussed also in Sect. 3.2. If we can neglect the effects

of the wire properties, then the analysis becomes simpler and convenient for direct determination of the thermal conductivity from the slope of the frequency response of the 3ω component. Therefore, the main objective of the present study is to clarify the conditions where wire properties can be neglected in the measurement of thermal conductivity and thermal diffusivity of hydrogen gas by the 3ω method.

2 Analytical Solution

The three-omega method uses a plated strip or wire that serves both as a heater and a thermometer. The frequency dependence of the temperature oscillations are used instead of the time-domain response in contrast to the conventional transient hot-wire method. Cahill [1] derived an analytical one-dimensional (1D) solution for a finite width strip heater plated onto a solid sample. For fluids, however, a micro-wire heater may be more convenient. Analytical relations for the 3ω voltage components arising from an oscillating current in a circular wire can be found, for example, in Griesinger et al. [13] and Wang et al. [5]. In the present study it is assumed that the aspect ratio L/D is large enough for neglecting end effects, and heat transfer by natural convection of sample is also negligible. Unsteady heat conduction in the sample ($r > r_o$) is governed by the following equation:

$$\frac{1}{r}\frac{\partial T}{\partial r} + \frac{\partial^2 T}{\partial r^2} - \frac{1}{\alpha}\left(\frac{\partial T}{\partial t}\right) = 0 \tag{1}$$

Neglecting the radial temperature gradient in the wire, the boundary condition at $r = r_o$ for Eq.1 is given by

1. omitting the wire heat capacity

$$-2\pi r_o l \lambda_s \frac{\partial T}{\partial r}\Big|_{r=r_o} = W \tag{1a}$$

2. including the wire heat capacity

$$-2\pi r_o l \lambda_s \frac{\partial T}{\partial r}\Big|_{r=r_o} = W - \pi r_o^2 l \left(\rho C_p\right)_w \frac{\partial T}{\partial t}\Big|_{r=r_o} \tag{1b}$$

For an oscillating electric current $I = I_o \cos(\omega t)$, the power, W to the wire is given by

$$W = I^2 R = I_o^2 R \cos^2(\omega t) = \frac{I_o^2 R}{2}(1 + \cos(2\omega t)) \tag{2}$$

where R is the electrical resistance of the wire. The other boundary condition for Eq. 1 is

$$T\,|_{r\to\infty} = 0 \tag{3}$$

Rather than using an initial condition, we assume that the time is large enough so that only steady oscillating terms remain in the solution. Also we neglect the transient effect of the direct current part of Eq. 2. By making the substitution, $T = ue^{i2\omega t}$, the following general solution to Eq. 1 in terms of Bessel functions can be obtained [14]:

$$u = Q_1 I_0(ar\mathrm{i}^{1/2}) + Q_2 K_0(ar\mathrm{i}^{1/2}); a = (2\omega/\alpha_\mathrm{s})^{1/2}$$

Eq. 3 gives $Q_1 = 0$.

If the boundary condition at $r = r_\mathrm{o}$ is applied and (following Cahill [1]) we make use of the assumption $|ar\mathrm{i}^{1/2}| \ll 1$, finally we obtain the temperature oscillation $T_{2\omega}$ in the frequency domain,

1. omitting the wire heat capacity

$$\begin{aligned} T_{2\omega} &= \left(\frac{I_\mathrm{o}^2 R_{T0}}{4\pi l \lambda_\mathrm{s}} A\right) \cos(2\omega t) + \left(\frac{I_\mathrm{o}^2 R_{T0}}{16 l \lambda_\mathrm{s}}\right) \sin(2\omega t) \\ A &= (-1/2 \ln(2\omega/\alpha_\mathrm{s}) - \ln(r_\mathrm{o}) - 0.5772 + \ln 2) \end{aligned} \tag{4}$$

2. including the wire heat capacity

$$\begin{aligned} T_{x-2\omega} &= \left(\frac{I_\mathrm{o}^2 R_{T0}}{2\pi l} \frac{A\lambda_\mathrm{s}}{\left(r_\mathrm{o}^2 \left(\rho C_p\right)_\mathrm{w} \omega A\right)^2 + (\pi r_\mathrm{o}^2 \left(\rho C_p\right)_\mathrm{w} \omega/4 + \lambda_\mathrm{s})^2}\right) \cos(2\omega t) \\ T_{y-2\omega} &= \left(\frac{I_\mathrm{o}^2 R_{T0}}{2\pi l} \frac{\left(A^2 + \frac{\pi^2}{16}\right) r_\mathrm{o}^2 \left(\rho C_p\right)_\mathrm{w} \omega + \frac{\pi\lambda_\mathrm{s}}{4}}{\left(r_\mathrm{o}^2 \left(\rho C_p\right)_\mathrm{w} \omega A\right)^2 + (\pi r_\mathrm{o}^2 \left(\rho C_p\right)_\mathrm{w} \omega/4 + \lambda_\mathrm{s})^2}\right) \sin(2\omega t) \end{aligned} \tag{5}$$

The current source input at a frequency ω induces temperature oscillations at the doubled frequency 2ω (Eqs. 4 and 5). This results in a voltage oscillation across the heating element that includes the tripled frequency components at 3ω, shown in Eqs. 7 and 8. To determine the voltage, the resistance of the probe is given as a function of the probe temperature via the equation,

$$R_{0\mathrm{C}} = \rho_{0\mathrm{C}} \frac{L}{\pi r^2}; R_T = R_{0\mathrm{C}}(1 + \beta(T_0 + T)); R_{T0} = R_{0\mathrm{C}}(1 + \beta T_0)$$

where $R_{0\mathrm{C}}$ is the resistance at 0 °C and β is the corresponding temperature coefficient of the wire. T_0 is the temperature in °C at the start of the experiment, and T is the temperature rise used in Eq. 1. Thus, the voltage is given by

$$V = I_0 \cos(\omega t) R_{0\mathrm{C}} (1 + \beta (T_0 + T_{2\omega})) \tag{6}$$

The 3ω components of the voltage will be

1. omitting the wire heat capacity:

$$V_{3\omega} = \left(\frac{I_o^3 R_{0C} R_{T0} \beta}{8\pi l \lambda_s}\right) A\cos(3\omega t) + \left(\frac{I_o^3 R_{0C} R_{T0} \beta}{32 l \lambda_s}\right) \sin(3\omega t) \tag{7}$$

2. including the wire heat capacity:

$$V_{3\omega X} = \left(\frac{I_o^3 R_{0C} R_{T0} \beta}{8\pi l} \frac{A\lambda_s}{\left(r_o^2 \left(\rho C_p\right)_w \omega A\right)^2 + (\pi r_o^2 \left(\rho C_p\right)_w \omega/4 + \lambda_s)^2}\right) \cos(3\omega t)$$

$$V_{3\omega Y} = \left(\frac{I_o^3 R_{0C} R_{T0} \beta}{8\pi l} \frac{\left(A^2 + \frac{\pi^2}{16}\right) r_o^2 \left(\rho C_p\right)_w \omega + \frac{\pi\lambda_s}{4}}{\left(r_o^2 \left(\rho C_p\right)_w \omega A\right)^2 + \left(\pi r_o^2 \left(\rho C_p\right)_w \omega/4 + \lambda_s\right)^2}\right) \sin(3\omega t) \tag{8}$$

where ρ_w and $(C_p)_w$ are the density and specific heat of the wire, respectively (Eq. 8). Note that Eq. 8 will approach to Eq. 7 if $(\rho C_p)_w \to 0$. The same condition will occur if the radius of the wire, r_o is reduced to a fine wire. To measure the thermal conductivity, the result can be obtained directly from Eq. 7 using the gradient of the voltage when plotted against the logarithm of the frequency. However, if the wire heat capacity is not negligible, determining λ and α for the sample becomes complicated since some kind of curve fitting procedure is needed for Eq. 8. Therefore, it is desirable to clarify the conditions for which it is safe to neglect the heat capacity of the wire.

3 Calculation Results

The above analytical one-dimensional solutions are used to simulate temperature oscillations over a range of frequencies. The aspect ratio (l/D) of the simulation is chosen to be about 2000 to reduce end effects without making the wire impractically long.The three-omega voltage component for water, toluene, air, and hydrogen is simulated. Figures 1 and 2 show simulations of a 10 µm platinum wire in water and toluene, respectively. A 10 µm diameter wire was selected since it is a practical size that is typically used in the transient hot-wire method.

3.1 Effect of Wire Heat Capacity

From Figs. 1 and 2 it is clear that the wire heat capacity does have an important effect on the frequency response of the 3ω components. In agreement with Wang et al. [5], Fig. 1 shows that the effect of the wire properties becomes greater as the frequency is increased. Comparing Figs. 1 and 2 it is also apparent that the effect of the wire heat capacity is greater for toluene than it is for water. As we will show below, this is because the thermal conductivity of water (about $0.6\,\mathrm{W \cdot m^{-1} \cdot K^{-1}}$) is greater than that of toluene ($0.13\,\mathrm{W \cdot m^{-1} \cdot K^{-1}}$). The smaller volumetric heat capacity of toluene also has an effect. Figures 3 and 4 show simulations for air and hydrogen, respectively. In contrast to the liquid cases, the heat capacity of the wire has a major effect

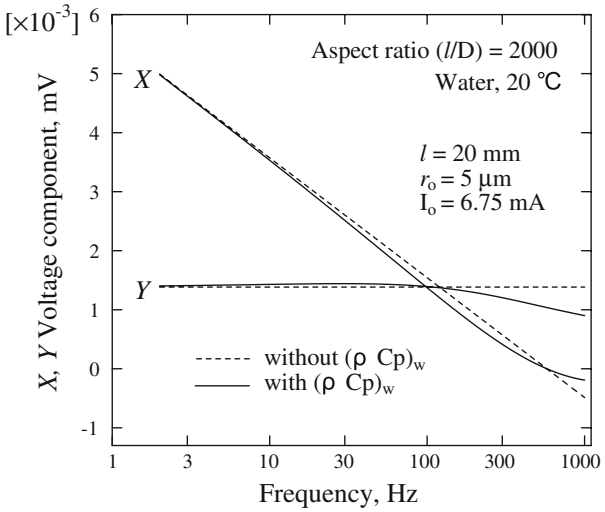

Fig. 1 Three-omega voltage component (*X*,*Y*) for water at 20 °C. Solid line includes wire heat capacity

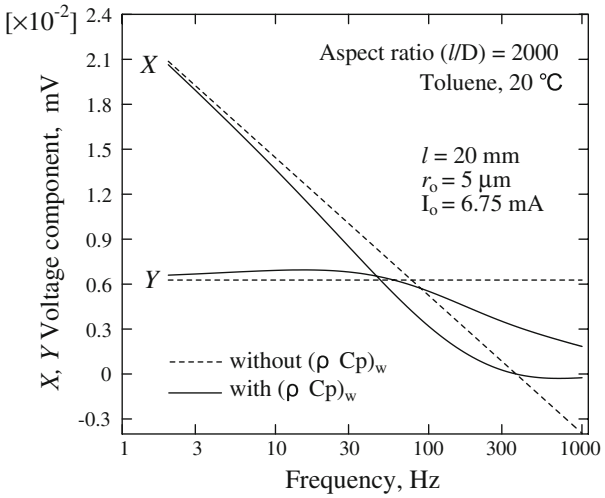

Fig. 2 Three-omega voltage components for toluene at 20 °C. Solid line includes wire heat capacity

on the 3ω components of the voltage. This is consistent with the results of Lee [9]. Rather than taking on an approximately constant value as in Eq. 7, the out-of-phase component, *Y*, from Eq. 8 has a clear peak in the cases of air and hydrogen shown in Figs. 3 and 4. Moreover, the in-phase component, *X*, is much lower than that predicted by Eq. 7 and rapidly extrapolates asymptotically to zero as the frequency is increased. Another interesting feature is that in the case of air the voltage is an order of magnitude larger than that of hydrogen for the same current (6.75 mA). Again this is due to the difference in thermal conductivity.

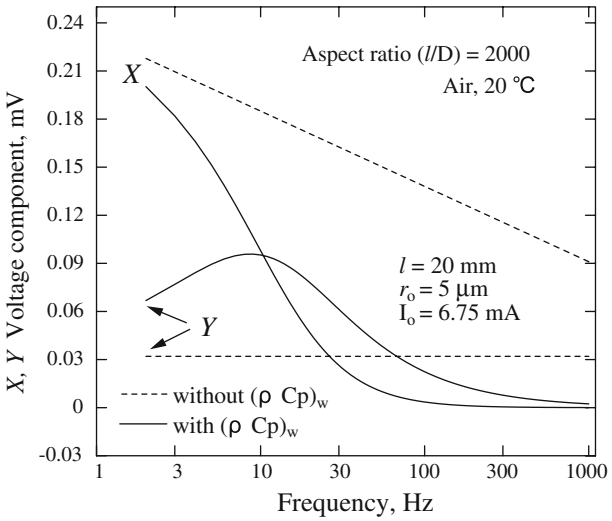

Fig. 3 Three-omega voltage component for air at 20 °C, 0.1013 MPa. Solid line includes wire heat capacity

From Figs. 1, 2, 3, and 4 it is confirmed that the wire heat capacity will have a very important influence on the results for gas-phase measurement. One may suppose that this is mostly due to the large difference between the heat capacity of the gas and the heat capacity of the wire. However, the volumetric heat capacity (ρC_p) of air at 20 °C and atmospheric pressure (1212 $J \cdot m^{-3} \cdot K^{-1}$) is similar to that of hydrogen (1200 $J \cdot m^{-3} \cdot K^{-1}$) for the same conditions and yet the effect of the wire heat capacity appears significantly greater in Fig. 3 for air than in Fig. 4 for hydrogen. Therefore, the thermal conductivity of the sample also plays an important role.

We can see that at low frequencies, the agreement between the result from Eq. 7 and that using Eq. 8 is better than at high frequencies. If we divide the coefficient of $\cos(3\omega t)$ in Eq. 7 by the coefficient of $\cos(3\omega t)$ in Eq. 8, we obtain

$$\frac{V_{3\omega X(\text{without}(\rho C_p)_w)}}{V_{3\omega X}} = \left(1 + \frac{\pi r_o^2 (\rho C_p)_w \omega}{4\lambda_s}\right)^2 + \left(\frac{r_o^2 (\rho C_p)_w \omega A}{\lambda_s}\right)^2 = 1 + C$$

where C is the change from unity of the ratio of the in-phase component with and without the wire heat capacity. In the limit where the dimensionless group $(r_o^2(\rho C_p)_w\omega)/\lambda_s$ is small, we have

$$C \approx \frac{\pi r_o^2 (\rho C_p)_w \omega}{2\lambda_s} \tag{9}$$

Equation 9 suggests that the maximum frequency for which Eq. 8 may be considered valid when applied to a probe of radius r_o and heat capacity $(\rho C_p)_w$ inserted in a fluid

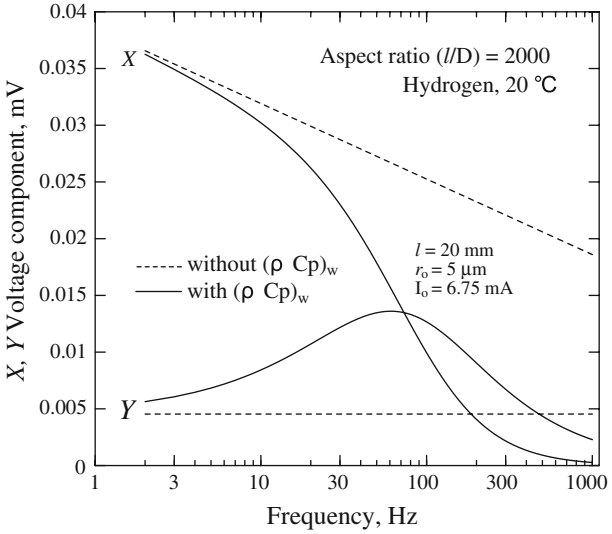

Fig. 4 Three-omega voltage component for hydrogen at 20 °C, 0.1013 MPa. Solid line includes wire heat capacity

of thermal conductivity λ is

$$f_{\max} = C_{\lim}\lambda_s / \left(\pi^2 r_o^2 \left(\rho C_p\right)_w\right) \tag{10}$$

In Eq. 10 $C_{\lim}$ should be understood as an allowable percentage error. The interesting feature of Eq. 10 is that it includes thermal conductivity but does not include the heat capacity of the sample. This confirms the above mentioned observation that the thermal conductivity of the sample plays an important role in determining whether or not the wire heat capacity may be neglected.

Both from Eq. 10 and from common sense we should expect that reducing the radius of the wire will reduce the effect of the wire heat capacity. Figures 5 and 6 show this effect where the 3ω components have been calculated for different wire diameters. Since the current is kept constant, the most obvious effect in Fig. 5 is the increase in the 3ω voltage for a decrease in the wire diameter. Another interesting feature in Fig. 5 is that the peak in the curve for the out-of-phase component Y shifts to higher frequencies with decreasing wire radius. The log-scale in Fig. 5 tends to hide the fact that the maximum allowable frequency for the case of $r_o = 3\,\mu m$ should be about 2.8 times that for $r_o = 5\,\mu m$ according to Eq. 10. The effect of the wire radius can be more clearly seen in Fig. 6 which shows calculations for micro-scale probe sensors of several different wire dimensions. From Fig. 6 it is apparent that the wire radius should be less than 1 m to obtain a straight line for the in-phase component, X, over a wide range of frequencies in hydrogen gas at atmospheric pressure.

Figure 7 shows calculations for a nano-scale sensor. It is apparent that for a wire of radius 25 nm, the linear section of the curve increases to frequencies well over $10^4 s^{-1}$. Since for higher frequencies, the 1D assumption may still be valid with a smaller aspect

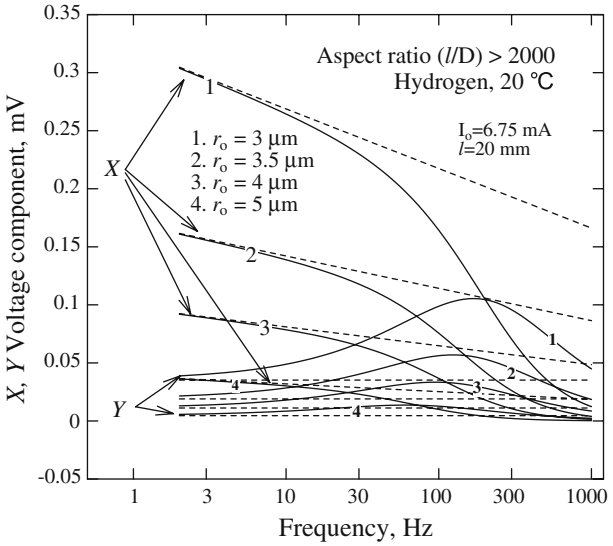

Fig. 5 Effect of the wire radius (dashed line without wire heat capacity and solid line includes wire heat capacity)

ratio, Fig. 7 also shows a case with an aspect ratio of l/D = 200. With the shorter wire and larger current, we can still obtain the same measured voltage. While Fig. 7 shows that the nano-scale probe definitely can remove the effect of the wire heat capacity it is a big challenge to develop such a nano-sensor experimentally. If such a nano-sensor can be realized practically, removing the wire heat capacity within this method gives new hope for measuring the hydrogen gas thermal conductivity at high pressure and high temperature accurately and safely in a very small pressure vessel.

Noting that the resistances R_T and R_{0C} are directly proportional to the length of the wire, we should expect from Eqs. 7 and 8 that the three-omega components of the voltage will increase in direct proportion to the length of the wire. This is confirmed in Fig. 8 which shows the components X and Y for different wire lengths while maintaining a constant current and wire diameter.

Equations 7 and 8 also show that the 3ω voltage components increase with the third power of the current. This is in contrast to the transient hot-wire method where the measured voltage of interest increases with the square of the current. The third power relationship implies that a very small increase in current can make a large difference to the magnitude of the measured 3ω components. Figure 9 illustrates this by showing that a 30 % increase in current from 6.75 mA to 8.75 mA makes the measured voltage more than double in magnitude.

Since Fig. 6 indicates that a 0.4 µm diameter probe may be suitable for hydrogen gas thermal-conductivity measurement, it is worthwhile to briefly consider the effect of applying such a probe to other gases. Equation 10 suggests that as the thermal conductivity of the gas decreases, the maximum allowable frequency will also decrease. Figure 10 shows calculation results for a micro-scale probe, 0.4 µm in diameter and 0.8 mm in length, applied to several gases. The gases are listed from 1 to 5

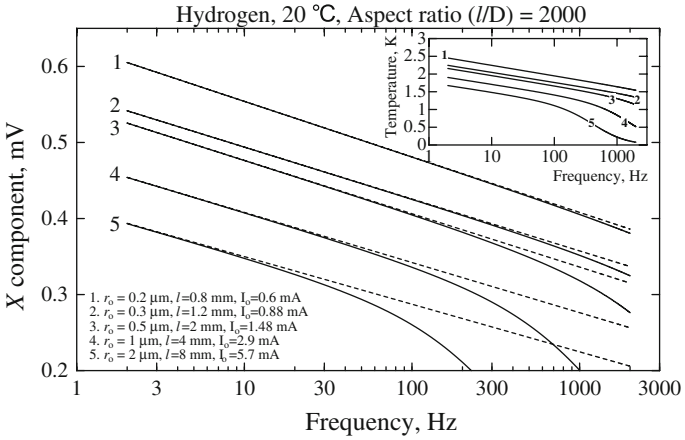

Fig. 6 Effect of reducing wire diameter from 4 µm to less than 1 µm applied for hydrogen gas (dashed line without wire heat capacity and solid line includes wire heat capacity)

in order of increasing molar mass. With the exception of air and N_2 (which have very similar properties), this also corresponds to the order of decreasing thermal conductivity. From Fig. 10 it can be seen that the maximum allowable frequency decreases in the order of decreasing thermal conductivity as expected from Eq. 10. With a probe of the dimensions given in Fig. 10 we could measure hydrogen and helium neglecting the wire heat capacity up to 1 kHz, for nitrogen and air up to 80 Hz, and for argon up to 40 Hz. In principle, both the out-of-phase component (Y) and in-phase component (X), could give the thermal conductivity and thermal diffusivity. However the in-phase component (X) has been found to be more reliable experimentally than the out-of-phase component (Cahill [1]). It should be noted here that the simulations above are using a one-dimensional analysis and confirmation of the validity of neglecting end effects is still required.

3.2 Temperature Jump Effects

Figures 6, 7 and 10 indicate that a hot wire suitable for gas thermal-conductivity measurements should have a small diameter. However, it may be anticipated that problems with the measurement will occur if the wire diameter or thermal penetration depth is comparable to the mean free path of the gas sample. A possible approach to compensate for such effects is to treat the bulk of the sample as a continuum and change the boundary condition at the gas/solid interface to allow for a discontinuity in temperature (e.g., Ref. [15]). In such a case, the boundary condition specified by Eq. 1a should be replaced by

$$-\lambda_s \frac{\partial T}{\partial r} = K_j \left(T_w - T|_{r=r_o}\right) \tag{11}$$

K_j can be estimated based on the kinetic theory of gases by

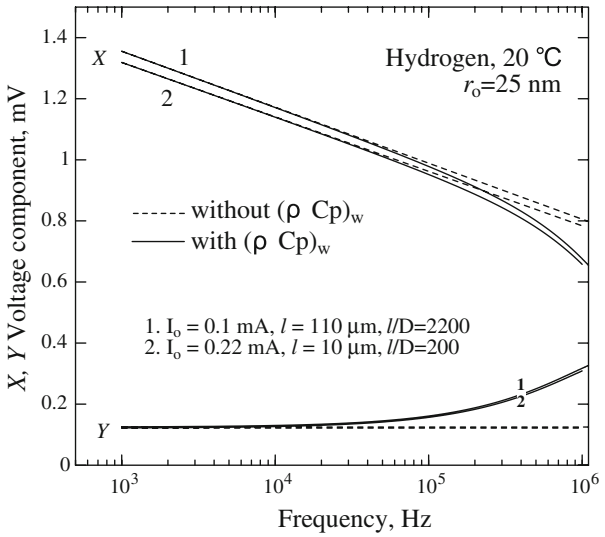

Fig. 7 Simulation for a nano-scale probe sensor

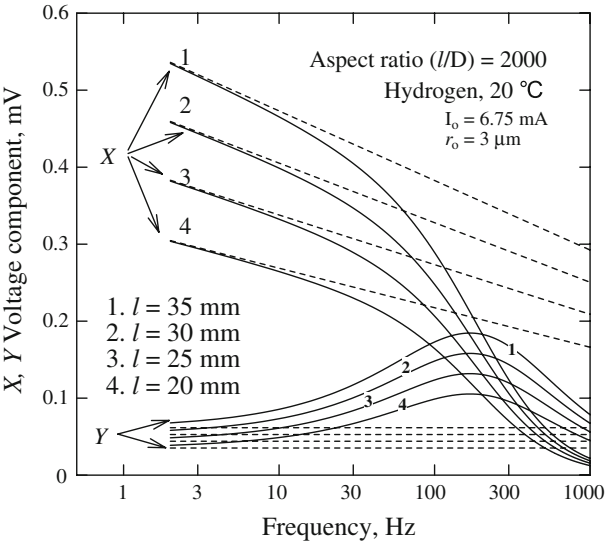

Fig. 8 Effect of wire length (dashed line without wire heat capacity and solid line includes wire heat capacity)

$$K_j = \frac{\lambda_s Pr}{2l_{mfp}} \frac{A_j}{(2 - A_j)} \left(\frac{\gamma_c + 1}{\gamma_c} \right) \tag{12}$$

A_j has a value of the order of unity [15]. The mean free path may be estimated using

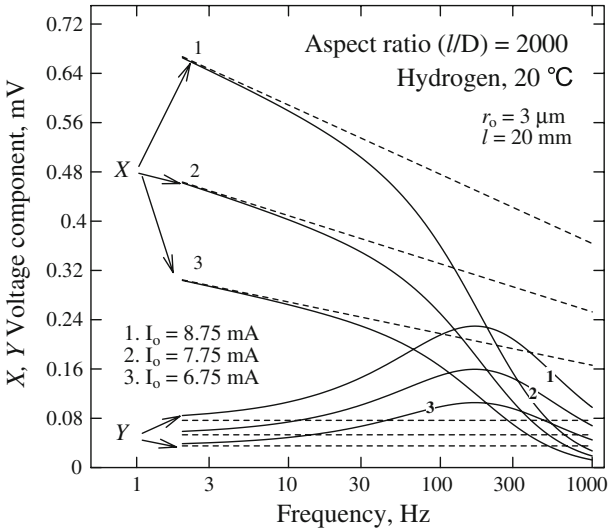

Fig. 9 Effect of changing the electrical current (dashed line without wire heat capacity and solid line includes wire heat capacity)

$$l_{\mathrm{mfp}} = \frac{kT}{\sqrt{2}\sigma P} \tag{13}$$

Using Eq. 11 for the case where the wire heat capacity is neglected, the resulting 3ω voltage is given by

$$V_{3\omega} = \left(V_{\mathrm{j}3\omega} + \left(\frac{I_{\mathrm{o}}^3 R_{0\mathrm{C}} R_{T0}\beta}{8\pi l \lambda_{\mathrm{s}}}\right) A\right) \cos(3\omega t) + \left(\frac{I_{\mathrm{o}}^3 R_{0\mathrm{C}} R_{T0}\beta}{32 l \lambda_{\mathrm{s}}}\right) \sin(3\omega t) \tag{14}$$

where

$$V_{\mathrm{j}3\omega} = \frac{I_{\mathrm{o}}^3 R_{0\mathrm{C}} R_{T0}\beta}{8\pi r_{\mathrm{o}} l K_{\mathrm{j}}} \tag{15}$$

It may be noted here that Eq. 14 is the same as Eq. 7 except for the term $V_{\mathrm{j}3\omega}$. Moreover, Eq. 15 does not depend on the angular frequency. Therefore the effect of the temperature jump (in the case where the wire heat capacity can be neglected) is to shift the in-phase 3ω voltage up by a constant amount given by Eq. 15. Thus, in principle, the temperature jump will not influence the measured thermal conductivity if it can be determined using the slope of the in-phase component against the logarithm of frequency. This result is consistent with Cahill's justification for neglecting the contact resistance between the heater element and the solid sample in his 3ω method [1]. However, we must keep in mind that Eq. 11 is only applicable in the 'slip' regime (small Knudsen numbers) [15]. For the cases where the wire heat capacity cannot be neglected and for the nano-scale probe in Fig. 7, further investigation may be needed. In any case, the validity of the present analysis will improve as the pressure is increased as can be

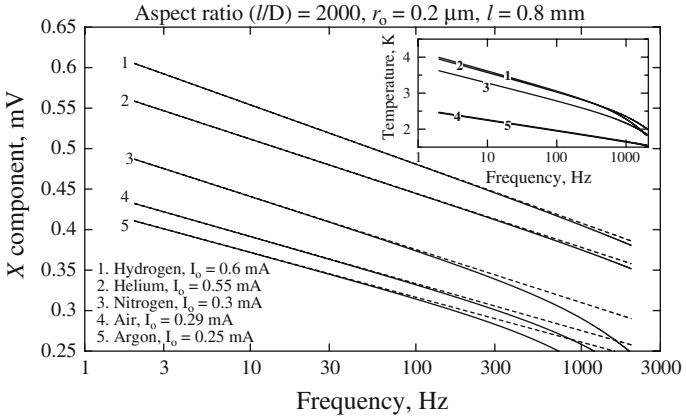

Fig. 10 Micro-scale-probe sensor applied for several gases (dashed line without wire heat capacity and solid line includes wire heat capacity)

deduced from Eq. 13. A full treatment of such considerations is beyond the scope of the present study, but is highly recommended as a subject of further experimental and theoretical research.

4 Preliminary Experiment

To validate the conclusions of the present article in relation to the effect of the wire heat capacity a preliminary experiment was carried out with a 10 μm diameter platinum wire approximately 15 mm long in a sealed container filled with air at atmospheric pressure and room temperature. Figure 11 shows the circuit used. The experiment was performed both with a lock-in-amp (Signal Recovery DSP Model 7265) and a two-channel 24 bit high speed analog/digital conversion board (National Instruments PXI-5922) for confirmation. In the case of the A/D board the three-omega components were extracted from the data using Fourier transforms applied over 0.8 s of data sampled at a rate of 50,000 samples per second. The sinusoidal signal to power the circuit was generated using a function generator (NF WF1974) with an internal resistance of $R_{\mathrm{fg}} = 50\,\Omega$. The reference signal for the lock-in-amp was taken from the voltage measured across a standard resistor of $R_{\mathrm{ref}} = 25\,\Omega$.

For a given voltage setting, the magnitude of the sinusoidal current was calculated from analysis of the circuit shown in Fig. 11 and confirmed by measuring the voltage across the reference resistor directly with one channel of the A/D board. The present circuit is simpler than that of Cahill [1] but has the disadvantage that the effect of the 3ω component of the current flowing through the circuit is not automatically subtracted. Note that Eqs. 4–8 above assume that the current contains no 3ω components and is simply given by $I = I_{\mathrm{o}} \cos(\omega t)$. Since the function generator in Fig. 11 produces an oscillating voltage rather than a pure oscillating current, the 3ω voltage component across the probe will in turn produce a 3ω component in the current. By neglecting higher-order terms, and assuming the case of a perfect signal

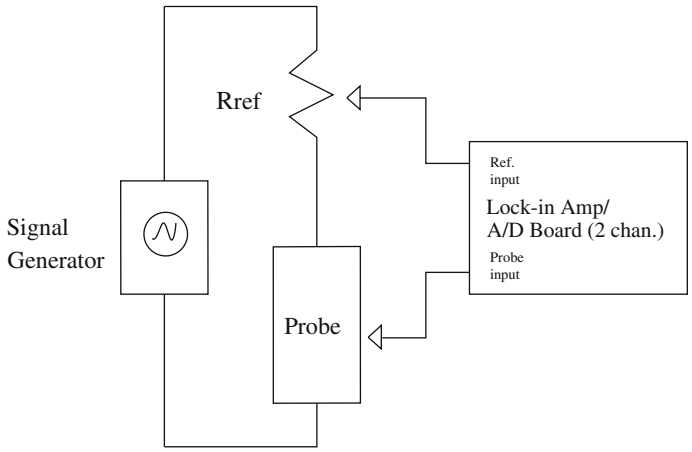

Fig. 11 Circuit arrangement for experiment

generator ($V_{\mathrm{fg}3\omega} = 0$), to correct for this difference between the model and the experiment, then the 3ω components given in Eqs. 7 and 8 need to be multiplied by the factor $\left(R_{\mathrm{fg}} + R_{\mathrm{ref}}\right) / \left(R_T + R_{\mathrm{fg}} + R_{\mathrm{ref}}\right)$ (see Appendix). Unlike Cahill's experimental method [1], this cannot correct for imperfections in the generated signal but this approach was considered to be of sufficient accuracy for the purpose of the present preliminary investigation.

Figure 12 shows comparison results of the preliminary experiment applied to air with the voltages calculated from Eqs. 7 and 8. The solid lines correspond to Eq. 8 which includes the wire heat capacity while the dashed lines correspond to Eq. 7. Note that the above-mentioned factor to correct for the effect of the 3ω component of the current in the experiment has been applied to the calculated voltage curves. The function generator was set at 1.2 V_{pp} for the example in Fig. 12a and at 2.4 V_{pp} for Fig. 12b. The 3ω components were measured for frequencies ranging from 5 Hz to 1,000 Hz.

In order to specify accurately the temperature at which the thermal conductivity is measured, it is desirable to keep the temperature rise of the wire less than 1 K. This is almost achieved for the case shown in Fig. 12a where from simulation, the mean temperature rise of the wire is calculated to be about 1.4 K over a period of 4 s. For the case in Fig. 12b the mean wire temperature rise is about 5.6 K over the same time period. Therefore, from the point of view of avoiding ambiguity in specifying the temperature, the smaller current is preferred. However, in general, the agreement between experiment and the present theory is much better for Fig. 12b than for Fig. 12a. For example, the measured values for X components in Fig. 12a become negative at frequencies greater than about 50 Hz and have a magnitude greater than that given by Eq. 8 (dashed line). The reason for the better agreement between theory and measurement in Fig. 12b is that the measured 3ω voltages in Fig. 12b are almost an order of magnitude larger than those in Fig. 12a. This is consistent with Eq. 8 which implies that doubling the magnitude of the oscillating current, I_{o}, leads to an increase in the 3ω voltages by a factor of eight.

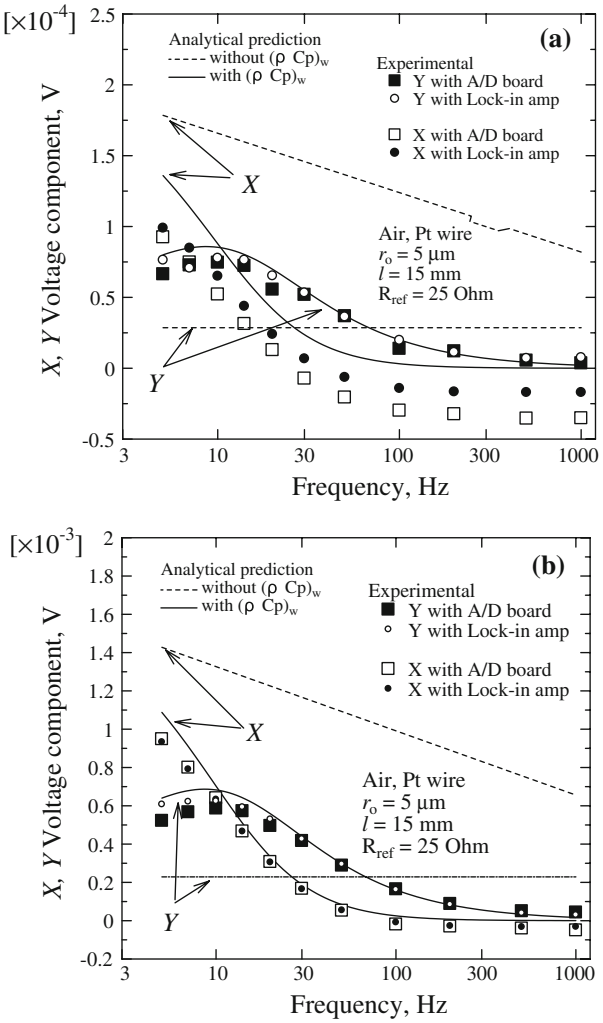

Fig. 12 Pre-experimental data obtained by Pt wire probe: (**a**) function generator: $0.6\cos(\omega t)$V and (**b**) function generator: $1.2\cos(\omega t)$V

In Fig. 12a the error in the measurement is mostly due to the fact that the signal generator is not perfect so that the output signal contains a third harmonic component. In the case of the A/D board data, we can determine the 3ω component of the current by performing a Fourier analysis of the measured voltage across the reference resistor shown in Fig. 11. Figure 13 shows the effect of subtracting the contribution of the measured 3ω current from the A/D board raw data for the in-phase component shown in Fig. 12a. Clearly from Fig. 13, the subtraction is quite effective in improving the agreement between the experimental data and the theory (Eq. 8). Subtracting the voltage due to the measured 3ω current through the reference resistor removes the need for the correction factor described in the Appendix and makes the procedure mathematically

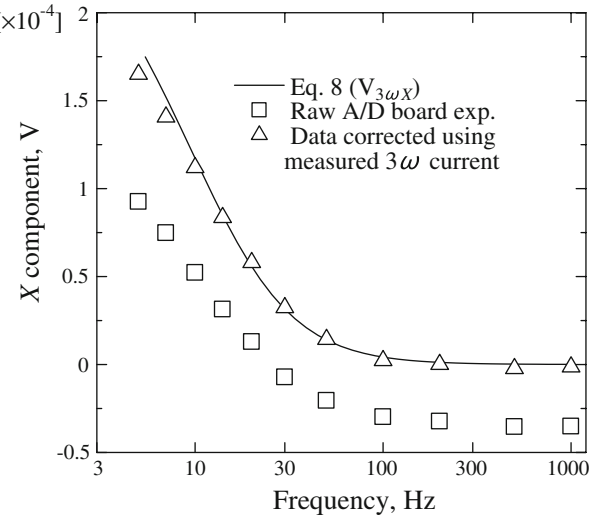

Fig. 13 Effect of subtracting the contribution of the measured 3ω component in the current from the raw data in Fig. 12a (X component, A/D board, 1.2 V_{pp})

equivalent to the experimental circuit used by Cahill [1]. Most importantly, it accounts for the 3ω components produced in the signal generator itself. Unfortunately, such a subtraction cannot be done with a lock-in-amp for the circuit in Fig. 11. Moreover, the large 1ω component can produce a distortion in the measured 3ω voltage in the lock-in-amp [1]. This may explain the difference between the readings for the lock-in-amp and the A/D board in Fig. 12. Therefore the circuit in Fig. 11 cannot be recommended for practical measurement of thermal conductivity with a lock-in-amp. Nonetheless, for all of the data collected, Eq. 8 is in much better agreement with the experiment than Eq. 7. Thus Fig. 12 confirms the importance of the heat capacity of the wire when applying the 3ω method to gases.

5 Conclusion

The measurement of thermal conductivity and thermal diffusivity with the 3ω method is more complicated for the gas phase than for the solid or liquid phases. The wire heat capacity should be considered carefully since the gas-phase properties are very different from those of the wire and gas often has a low thermal conductivity. Based on this present study, to determine the thermal conductivity of hydrogen gas with direct measurement of the 3ω voltage gradient in the frequency domain, a small diameter wire probe with a large aspect ratio is recommended. For a practical micro-scale wire probe, in order to neglect the heat capacity, it may be possible to take measurements at frequencies up to 10 Hz. However, low frequencies are undesirable because of the increasing influence of end effects, natural convection, and the higher penetration depth into the sample. Increasing the length of the wire is useful to increase the magnitude of the 3ω voltage components and aspect ratio of the probe. A nano-scale probe

definitely could remove the effect of the wire heat capacity; however, experimentally there are many challenges. In principle, the temperature jump will not influence the measured thermal conductivity if it can be determined using the slope of the in-phase component against the logarithm of frequency. However, for cases where the wire heat capacity cannot be neglected and for the nano-scale probe, further investigation into rarefied gas effects may be needed. The three-omega method may be a useful tool for such a study. Moreover, the results mentioned above are from a one-dimensional analysis and confirmation of the validity of neglecting end effects is also required.

Acknowledgments This research has been conducted as a part of the "Fundamental Research Project on Advanced Hydrogen Science" funded by New Energy and Industrial Technology Development Organization (NEDO).

Appendix: Approximate Analysis of Experimental Circuit

The theory used in deriving Eqs. 7 and 8 assumes that the electrical current contains no 3ω components and is given simply by $I_o \cos(\omega t)$. For the circuit in Fig. 11 this is not achieved since in principle, the signal generator produces an oscillating voltage, not a pure oscillating current. Moreover, since no signal generator is perfect, the output voltage from the signal generator will also contain three-omega components ($V_{fg3\omega} \cos(3\omega t + \phi)$). For simplicity, let us assume that the measured voltage across the probe is given by

$$V_p = V_{1\omega X} \cos(\omega t) + V_{1\omega Y} \sin(\omega t) + V_{3\omega X} \cos(3\omega t) + V_{3\omega Y} \sin(3\omega t) \quad \text{(A.1)}$$

Therefore, the current flowing through the circuit is given by

$$\begin{aligned} I &= \frac{V_{fg} \cos(\omega t) + V_{fg3\omega} \cos(3\omega t + \phi) - V_p}{R_{fg} + R_{ref}} \\ &\approx I_o \cos(\omega t) + \frac{V_{fg3\omega} \cos(3\omega t + \phi)}{R_{fg} + R_{ref}} - \frac{V_{1\omega Y} \sin(\omega t)}{R_{fg} + R_{ref}} \\ &\quad - \frac{V_{3\omega X} \cos(3\omega t)}{R_{fg} + R_{ref}} - \frac{V_{3\omega Y} \sin(3\omega t)}{R_{fg} + R_{ref}} \end{aligned} \quad \text{(A.2)}$$

where V_{fg} and R_{fg} are the voltage magnitude setting and internal resistance of the function generator, respectively. If we assume that the terms involving $\sin(\omega t)$, $\cos(3\omega t)$, and $\sin(3\omega t)$ contribute very little toward heating the wire, then the main change to the analysis is to replace $I_o \cos(\omega t)$ in Eq. 6 with Eq. A.2.

$$\begin{aligned} V &= I_o \cos(\omega t)\, R_{0C} (1 + \beta (T_0 + T_{2\omega})) + \frac{R_T V_{fg3\omega} \cos(3\omega t + \phi)}{R_{fg} + R_{ref}} \\ &\quad - \frac{R_T V_{1\omega Y} \sin(\omega t)}{R_{fg} + R_{ref}} - \frac{R_T V_{3\omega X} \cos(3\omega t)}{R_{fg} + R_{ref}} - \frac{R_T V_{3\omega Y} \sin(3\omega t)}{R_{fg} + R_{ref}} \end{aligned} \quad \text{(A.3)}$$

If for example, we consider the case without heat capacity and substitute Eq. 4 into Eq. A.3 and then evaluate the in-phase component of the 3ω voltage, we obtain

$$V_{3\omega X} = \frac{-R_T}{R_{\mathrm{fg}} + R_{\mathrm{ref}}} V_{3\omega X} + \frac{I_{\mathrm{o}}^3 R_{0\mathrm{C}} R_{T0} \beta A}{8\pi l \lambda} + \frac{R_T V_{\mathrm{fg}3\omega} \sin\phi}{R_{\mathrm{fg}} + R_{\mathrm{ref}}}$$

which may be arranged to give

$$V_{3\omega X} = \frac{R_{\mathrm{fg}} + R_{\mathrm{ref}}}{R_T + R_{\mathrm{fg}} + R_{\mathrm{ref}}} \times \left(\frac{I_{\mathrm{o}}^3 R_{0\mathrm{C}} R_{T0} \beta A}{8\pi l \lambda} + \frac{R_T V_{\mathrm{fg}3\omega} \sin\phi}{R_{\mathrm{fg}} + R_{\mathrm{ref}}} \right) \tag{A.4}$$

Thus for the circuit in Fig. 11, the 3ω components in Eqs. 7 and 8 should be multiplied by the factor $\left(R_{\mathrm{fg}} + R_{\mathrm{ref}}\right) / \left(R_T + R_{\mathrm{fg}} + R_{\mathrm{ref}}\right)$ even for the case of a perfect signal generator ($V_{\mathrm{fg}3\omega} = 0$). In the case of a real signal generator ($V_{\mathrm{fg}3\omega} \neq 0$), the result will be in error by the amount corresponding to the second term in the brackets in Eq. A.4.

References

1. D.G. Cahill, Rev. Sci. Instrum. **61**, 802 (1990)
2. D.G. Cahill, M. Katiyar, J.R. Abelson, Phys. Rev. B **50**, 6077 (1994)
3. S.M. Lee, D.G. Cahill, J. Appl. Phys. **81**, 2590 (1997)
4. T.Y. Choi, D. Poulikakos, App. Phys. Lett. **87**, 013108 (2005)
5. Z.L. Wang, D.W. Tang, S. Liu, X.H. Zheng, A. Araki, Int. J. Thermophys. **28**, 1255 (2007)
6. S.R. Choi, J. Kim, D. Kim, Rev. Sci. Instrum. **78**, 084902 (2007)
7. I.K. Moon, Y.H. Jeong, Rev. Sci. Instrum. **67**, 29 (1996)
8. N.O. Birge, Phys. Rev. B **34**, 3 (1986)
9. S.M. Lee, in *Proceedings 26th Japan Symp. Thermophysical Properties*, 2005, p. 44
10. F. Chen, J. Shulman, Y. Xue, C.W. Chu, Rev. Sci. Instrum. **75**, 4578 (2004)
11. N. Sakoda, E. Yusibani, P.L. Woodfield, K. Shinzato, M. Kohno, Y. Takata, M. Fujii, in *Proceedings 8th ATPC*, Fukuoka, Japan, paper no. 178 (2007)
12. M. Fujii, X. Zhang, N. Imaishi, S. Fujiwara, T. Sakamoto, Int. J. Thermophys. **18**, 327 (1997)
13. A. Griesinger, W. Heidemann, E. Hahne, Int. Commun. Heat Mass Transf. **26**, 451 (1999)
14. H.S. Carslaw, J.C. Jaeger, *Conduction of Heat in Solids*, 2nd edn. (Oxford University Press, London, 1959)
15. W.M. Rohsenow, H.Y. Choi, *Heat, Mass and Momentum Transfer* (Prentice-Hall, Englewood Cliffs, New Jersey, 1961)